# Catalytic Roles of Arginine Residues 82 and 92 of *Escherichia coli* 6-Hydroxymethyl-7,8-dihydropterin Pyrophosphokinase: Site-Directed Mutagenesis and Biochemical Studies†

Yue Li,‡ Yan Wu,‡ Jaroslaw Blaszczyk,§ Xinhua Ji,§ and Honggao Yan*,‡

*Department of Biochemistry and Molecular Biology, Michigan State University, East Lansing, Michigan 48824, and Macromolecular Crystallography Laboratory, National Cancer Institute, P.O. Box B, Frederick, Maryland 21702*

*Received September 4, 2002; Revised Manuscript Received December 6, 2002*

ABSTRACT: The roles of a pair of conserved positively charged residues R82 and R92 at a catalytic loop of *Escherichia coli* 6-hydroxymethyl-7,8-dihydropterin pyrophosphokinase (HPPK) have been investigated by site-directed mutagenesis and biochemical analysis. In the structure of HPPK in complex with ATP and a 6-hydroxymethyl-7,8-dihydropterin (HP) analogue, the guanidinium group of R82 forms two hydrogen bonds with the α-phosphate and that of R92 two hydrogen bonds with the *β*-phosphate. In the structure of HPPK in complex with α,*β*-methyleneadenosine triphosphate (AMPCPP, an ATP analogue) and HP, the guanidinium group of R82 has no direct interaction with AMPCPP and that of R92 forms two hydrogen bonds with the α-phosphate. Substitution of R82 with alanine caused a decrease in the rate constant for the chemical step by a factor of ∼380, but there were no significant changes in the binding energy or binding kinetics of either substrate. Substitution of R92 with alanine caused a decrease in the rate constant for the chemical step by a factor of $\sim 3.5 \times 10^4$. The mutation caused no significant changes in the binding energy or binding kinetics of MgATP. It did not cause a significant change in the binding energy of HP either but caused a decrease in the association rate constant for the binding of HP by a factor of ∼4.5 and a decrease in the dissociation rate constant by a factor of ∼10. The overall structures of the ternary complexes of both mutants were very similar to the corresponding structure of wild-type HPPK as described in the companion paper. The results suggest that R82 does not contribute to the binding of either substrate, and R92 is dispensable for the binding of MgATP but plays a role in facilitating the binding of HP. Both R82 and R92 are important for catalysis, and R92 plays a critical role in the transition state stabilization.

6-Hydroxymethyl-7,8-dihydropterin pyrophosphokinase (HPPK)[1] catalyzes the transfer of pyrophosphate from ATP to 6-hydroxymethyl-7,8-dihydropterin (HP, Figure 1), the first reaction in the folate biosynthetic pathway (*1*). Folate cofactors are essential for life (*2*). Mammals have an active transport system for deriving folates from the diet. In contrast, most microorganisms must synthesize folates de novo because they lack the active transport system. Therefore, like other enzymes in the folate biosynthetic pathway, HPPK is an attractive target for developing antimicrobial agents.

HPPK belongs to a class of enzymes that catalyze pyrophosphoryl transfer (*3*, *4*). While phosphoryl transfer reactions catalyzed by kinases take place at the *γ*-phosphorus of nucleoside triphosphate (NTP), pyrophosphoryl transfer reactions catalyzed by pyrophosphokinases takes place at the *β*-phosphorus of NTP. Nucleophilic substitution at the electron-rich *β*-phosphorus is thought to be more difficult than that at the *γ*-phosphorus; therefore, the enzymes that catalyze pyrophosphoryl transfer have lower $k_{cat}$ values (*4*). Kinases have been intensely studied for decades with respect to both structure and mechanism, but structural and mechanistic studies of pyrophosphokinases have just begun in earnest in recent years. Three-dimensional structures have

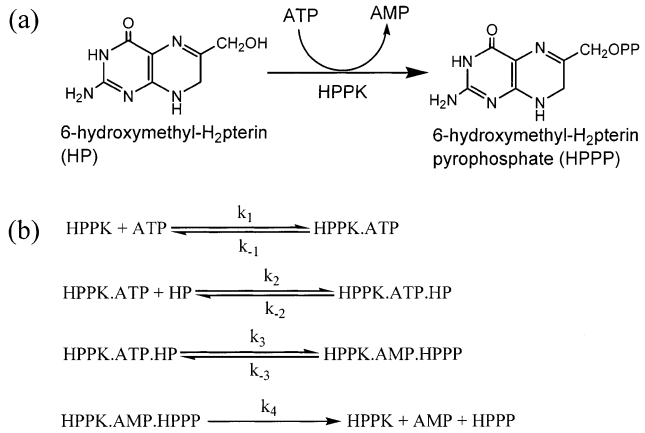


FIGURE 1: Pyrophosphoryl transfer reaction catalyzed by HPPK (a) and kinetic mechanism (b). $Mg^{2+}$ is required for the reaction, but for simplicity, $Mg^{2+}$ is not shown in the kinetic scheme.

† This work was supported in part by NIH Grant GM51901 (H.Y.).

* To whom correspondence should be addressed. Tel.: (517) 353-8786. Fax: (517) 353-9334. E-mail: yanh@msu.edu.

‡ Michigan State University.

§ National Cancer Institute.

[1] Abbreviations: AMPCPP, α,*β*-methyleneadenosine triphosphate; Ant-ATP, 3′(2′)-*O*-anthraniloyladenosine 5′-triphosphate; HPPK, 6-hydroxymethyl-7,8-dihydropterin pyrophosphokinase; HP, 6-hydroxymethyl-7,8-dihydropterin; NTP, nucleoside triphosphate; HPO, 6-hydroxymethylpterin; GST, glutathione S-transferase.

10.1021/bi026800z CCC: $25.00 
Published on Web 01/21/2003

been reported for phosphoribosyl diphosphate synthetase (*5*) and thiamine pyrophosphokinase (*6*, *7*) in addition to HPPK by us (*8*−*11*) and other groups (*12*, *13*). Most recently, we have shown by transient kinetic analysis that the chemical step is not rate-limiting in the reaction catalyzed by HPPK and that the low $k_{cat}$ value of HPPK reflects the slow release of the products rather than the true catalytic power of the enzyme (*14*). The thermodynamic and kinetic framework derived from the work has provided the foundation for dissecting the roles of active site residues in substrate binding and catalysis.

The structures of the ternary complexes of HPPK with a substrate and a substrate analogue have revealed the atomic maps for the possible interactions between the substrates and the enzyme (*9*, *13*). Among the active site residues revealed by the structures are R82 and R92. The two residues delimit a loop that undergoes a dramatic conformational change upon the formation of the ternary complexes. In the structure of HPPK in complex with an ATP analogue (AMPCPP) and HP (*9*), the guanidinium group of R82 forms two hydrogen bonds with the carboxylate of the conserved E77 but none with AMPCPP. The guanidinium group of R92 forms two hydrogen bonds with the α-phosphate of AMPCPP. In the structure of HPPK in complex with ATP and an HP analogue (*13*), the guanidinium group of R82 forms two hydrogen bonds with the α-phosphate of ATP and one hydrogen bond with the carboxylate of the conserved D95 that is coordinated with both bound $Mg^{2+}$ ions. The guanidinium group of R92 forms two hydrogen bonds with the *β*-phosphate of ATP. The structural information suggests that the two arginine residues may be important for substrate binding and/or catalysis. To investigate the roles of the two active site residues in substrate binding and catalysis, we have substituted the two residues, separately, with alanine by site-directed mutagenesis. In this paper, we describe the mutagenesis and biochemical studies of the roles of the two residues in the catalytic cycle. In the companion paper, we describe a 0.89 Å crystal structure of a ternary complex of the wild-type HPPK and crystallographic analysis of the two site-directed mutants.

## EXPERIMENTAL PROCEDURES

*Materials.* ATP and AMPCPP were purchased from Sigma. 6-Hydroxymethylpterin (HPO) was synthesized according to Thijssen (*15*) and had the same UV absorption and NMR spectra as that purchased from Sigma. HP was prepared from HPO by reduction with sodium dithionite (*16*) or purchased from Schircks Laboratories.

*Mutant Construction and Protein Purification*. The site-directed mutants were made by a PCR-based method using high-fidelity *pfu* DNA polymerase according to a protocol developed by Stratagene. The forward and reverse primers for making the R82A mutant were 5′-GAATTGCA GCAAGGTGCCGTCCGCAAAGCTGAACGC-3′and 5′-GCGTTCAGCTTTGCGGACGGCA CC TTGCTGCAATTC-3′, respectively. The forward and reverse primers for making the R92A mutant were 5′-GAACGCTGGGGACCAGCCACG CTGGATCTCGAC-3′and 5′-GTCGAGA TCCAGCGTG G CTGGTCCCCAGCGTTC-3′, respectively. The mutant was selected by DNA sequencing. To ensure that there were no unintended mutations in the mutant, the entire sequence of the mutated gene was determined. The proteins of the two mutants were purified as previously described for the wild-type enzyme (*17*).

*Construction and Purification of HPPK*−*GST Fusion*. The HPPK genes were subcloned into the *Nde* I and *Bam*H I sites of an expression vector (pET14b-3T) derived from the Novagen vector pET14b. HPPK was fused to glutathione S-transferase (GST) with a link that included a thrombin cleavage site. The fusion proteins were purified with a glutathione agarose column and digested with thrombin. The thrombin-digested proteins were run through a Sephadex G-75 column. The HPPK fractions were located by SDS−PAGE and concentrated by an Amicon cell with a YM10 membrane disk.

*Thermodynamic Analysis.* The $K_d$ values for various ligands were measured by fluorometric titration at 24 °C on a Spex FluoroMax-2 fluorometer as previously described (*14*, *17*). The titration experiments were performed in a single cuvette so that both protein and ligand concentrations varied with the addition of each aliquot of a stock solution. The independent variable in such an experiment was the volume of the added stock solution. The concentrations of the protein and the ligands during the titration could be expressed in terms of the initial concentrations of the titrated solution, the concentration of the stock solution, and the volume of the added stock solution. When HPPK was titrated with a ligand, the concentrations of HPPK ($E_t$) and the ligand ($L_t$) were varied according to the following expressions:

$$E_t = \frac{E_0 V_0}{V_0 + \Delta V}$$

$$L_t = \frac{L_0 \Delta V_0}{V_0 + \Delta V}$$

where $E_0$ is the initial concentration of HPPK, and $L_0$ is the concentration of the ligand stock solution. When a ligand was titrated with HPPK, the concentrations of HPPK and the ligand were varied according to the following expressions:

$$E_t = \frac{E_0 \Delta V_0}{V_0 + \Delta V}$$

$$L_t = \frac{L_0 V_0}{V_0 + \Delta V}$$

where $E_0$ is the concentration of the HPPK stock solution, and $L_0$ is the initial concentration of the ligand.

To determine the dissociation constant of Ant-ATP, 3 $\mu$M HPPK was titrated with Ant-ATP in 100 mM Tris-HCl and 10 mM $MgCl_2$, pH 8.3 (*17*). A set of control data was obtained in the absence of HPPK. The data set obtained in the absence of HPPK was then subtracted from the corresponding data set obtained in the presence of HPPK after correcting inner filter effects. The dissociation constant for Ant-ATP was obtained by nonlinear least-squares fit of the subtracted data using the program Origin (Microcal) to the following equation:

$$\Delta F_{obs} = \frac{\Delta F_{mol}(K_d + E_t + L_t - \sqrt{(K_d + E_t + L_t)^2 - 4E_tL_t})}{2} \quad (1)$$

where $\Delta F_{obs}$ and $\Delta F_{mol}$ are observed and molar fluorescence changes caused by binding, $E_t$ is the total concentration of HPPK, and $L_t$ is the total concentration of MgAnt−ATP.

The dissociation constants for nonfluorescent nucleotides were measured by a competitive binding assay as previously described (*14*). Briefly, a 2 mL solution containing 2 $\mu$M HPPK and 2 $\mu$M Ant-ATP in 100 mM Tris-HCl and 10 mM $MgCl_2$, pH 8.3, was titrated with AMPCPP at 24 °C. The fluorometric data were fitted by a nonlinear least-squares method using the program Origin to eq 2 derived by Wang (*18*).

$$F_{obs} = \epsilon_f A + \frac{(\epsilon_b - \epsilon_f)A\{2\sqrt{(a^2 - 3b)}\cos(\theta/3) - a\}}{3K_A + 2\sqrt{(a^2 - 3b)}\cos(\theta/3) - a} \quad (2)$$

where $\epsilon_f$ and $\epsilon_b$ are the molar fluorescence intensities for free and bound MgAnt−ATP, respectively, A is the concentration of Ant-ATP, and $K_A$ is the dissociation constant for MgAnt−ATP. Parameters $a$, $b$, and $\theta$ are defined by the following expressions:

$$a = K_A + K_B + A + B - P$$

$$b = K_A(B - P) + K_B(A - P) + K_AK_B$$

$$\theta = \arccos\left(\frac{-2a^3 + 9ab + 27K_AK_B}{2\sqrt{(a^2 - 3b)^3}}\right)$$

where B and P are the concentrations of a nonfluorescent nucleotide and HPPK, respectively, and $K_B$ is the dissociation constant for the nonfluorescent nucleotide.

To determine the $K_d$ value for HP, a 2 mL solution containing 0.11 $\mu$M HP and 100 $\mu$M AMPCPP in 50 mM BICINE, 10 mM $MgCl_2$, and 25 mM DTT, pH 8.3, was titrated with HPPK (*14*). The concentration of the HPPK stock solution was 20 $\mu$M. The final concentrations of HP and HPPK were 0.10 and 1.4 $\mu$M, respectively. A control titration experiment was performed in the absence of HP. The control data set obtained in the absence of HP was subtracted from the corresponding data set obtained in the presence of HP. The data were then fitted to the following equation:

$$F_{obs} = \frac{F_f\Delta V}{V_0 + \Delta V} + \frac{(F_b - F_f)(K_d + E_t + L_t - \sqrt{(K_d + E_t + L_t)^2 - 4E_tL_t})}{2L_t} \quad (3)$$

where $F_f$ and $F_b$ are the fluorescence intensities of free and bound HP, respectively, $F_{obs}$ is the fluorescence of each titration point, $V_0$ is the initial volume of the titration, $\Delta V$ is the total volume of the added HPPK solution, $E_t$ is the total concentration of HPPK, and $L_t$ is the total concentration of HP.

*Stopped-Flow Analysis*. Stopped-flow experiments were performed in an Applied Photophysics SX.18MV-R stopped-flow spectrofluorometer as previously described (*14*). To measure the binding of MgATP, a solution containing HPPK was mixed rapidly with a solution containing ATP and $MgCl_2$ at 25 °C. HPPK and $MgCl_2$ were fixed at 2 $\mu$M and 10 mM, respectively. ATP was varied from 2.5 to 20 $\mu$M. To measure the binding of MgAMPCPP, a solution containing HPPK was mixed rapidly with a solution containing AMPCPP, $MgCl_2$, and HP at 25 °C. HPPK, HP, and $MgCl_2$ were fixed at 1 $\mu$M, 20 $\mu$M, and 10 mM, respectively. AMPCPP was varied from 5 to 40 $\mu$M. To measure the binding of HP, a solution containing HPPK, AMPCPP, and $MgCl_2$ was mixed rapidly with a solution containing HP at 25 °C. HPPK, AMPCPP, and $MgCl_2$ were fixed at 0.2 $\mu$M, 25 $\mu$M, and 10 mM, respectively. HP was varied from 0.125 to 1 $\mu$M. All concentrations referred to the concentrations right after the rapid mixing. The rate constants were evaluated by numerical analysis of the stopped-flow data using the program DYNAFIT (*19*). The initial values for the iterative numerical analysis were obtained by nonlinear least-squares fit of the stopped-flow data to an exponential equation using the program Origin.

*Quench-Flow Analysis.* All quench-flow experiments were carried out with a KinTek RQF-3 rapid quench-flow instrument as previously described (*14*). All reaction components were dissolved in 100 mM Tris-HCl buffer, pH 8.3. A trace amount of [α-$^{32}$P]-ATP was used to follow the reactions. The reactions were initiated with $Mg^{2+}$ at 30 °C and quenched with 500 mM EDTA. The substrates and products were separated by thin-layer chromatography on a plastic sheet coated with PEI-cellulose developed with 0.25 M $NaH_2PO_4$. The radioactivity was quantified by a Molecular Dynamics Storm 820 Phosphor-Imager. In presteady-state experiments, the reaction mixture contained 10 $\mu$M HPPK, 100 $\mu$M ATP, 110 $\mu$M HP, 25 mM DTT, 0.5 mM EDTA, and 10 mM $MgCl_2$ in 100 mM Tris-HCl buffer, pH 8.3. The presteady-state data were first analyzed by nonlinear least-squares fit of the data to eq 4. The amplitudes and rate constants were then used to set the initial values for fitting the data to the complete mechanism by numerical analysis using the program DYNAFIT (*19*).

$$[AMP]/[HPPK] = A(1 - e^{\lambda}t) + k_{cat}t \quad (4)$$

## RESULTS

*Thermodynamic Analysis.* The HPPK-catalyzed reaction apparently follows an ordered bi-bi mechanism (*20*). Previously, we established a thermodynamic and kinetic framework for the reaction by a combination of thermodynamic and transient kinetic analysis (Figure 1 and Tables 1 and 2) (*14*). The same approach was used for the characterization of the mutants. The equilibrium binding properties were measured by fluorometric titration. The dissociation constant of MgAnt−ATP, a fluorescent analogue of MgATP, was determined by measuring the change in fluorescence upon the formation of the complex of MgAnt−ATP and HPPK, and those of other nucleotides were determined by a

Table 1: Ligand Binding Properties of Wild-Type HPPK and Mutants

| | WT | R82A | R92A |
|---|---|---|---|
| $K_{d(MgAntATP)}$ ($\mu$M) | 1.6 ± 0.05 | 1.7 ± 0.04 | 1.7 ± 0.01 |
| $K_{d(MgATP)}$ ($\mu$M) | 2.6 ± 0.06[a] | 3.9 ± 0.2 | 4.1 ± 0.04 |
| $K_{d(MgAMPCPP)}$ ($\mu$M) | 0.077 ± 0.006[b] | 0.11 ± 0.002 | 0.096 ± 0.005 |
| $K_{d(AMP)}$ ($\mu$M) | 140 ± 10[a] | 180 ± 10 | 440 ± 10 |
| $K_{d(HP)}$ ($\mu$M) | 0.17 ± 0.01[b] | 0.18 ± 0.004 | 0.084 ± 0.007 |

[a] From Shi et al. (*17*). [b] From Li et al. (*14*).

Table 2: Kinetic Parameters of Wild-Type HPPK and Variants

| | WT[a] | WT* [c] | R82A | R92A |
|---|---|---|---|---|
| $k_1$ ($\mu$M s$^{-1}$) | 0.27 ± 0.001 | | | 0.21 ± 0.001 |
| | 0.3 ± 0.02[b] | | 0.22 ± 0.02[b] | |
| $k_{-1}$ (s$^{-1}$) | 0.95 ± 0.001 | | | 0.88 ± 0.02 |
| | 0.023 ± 0.002[b] | | 0.02 ± 0.002[b] | |
| $k_2$ ($\mu$M s$^{-1}$) | 11 ± 0.03 | | 9.4 ± 0.04 | 2.5 ± 0.01 |
| $k_{-2}$ (s$^{-1}$) | 2.0 ± 0.04 | | 2.0 ± 0.01 | 0.2 ± 0.008 |
| $k_3$ (s$^{-1}$) | 16 ± 1 | 25 ± 2 | 0.066 ± 0.02[d] | (7.2 ± 0.09) × $10^{-4}$ [d] |
| $k_{-3}$ (s$^{-1}$) | 20 ± 1 | 27 ± 4 | | |
| $k_4$ (s$^{-1}$) | 1.8 ± 0.1 | 1.3 ± 0.1 | | |
| $k_{cat}$ (s$^{-1}$) | 0.76 | 0.61 | | |

[a] From Li et al. (*14*). [b] Measured for MgAMPCPP, this paper. [c] WT*, wild-type HPPK with four extra residues Gly−Ser−His−Met at the N-terminus. [d] Measured for R82A* or R92A* with four extra residues Gly−Ser−His−Met at the N-terminus.

competitive binding assay measuring the fluorescent changes caused by the displacement of MgAnt−ATP by the other nucleotides (Figures 2a and 3a). The dissociation constant of HP was measured in the presence of MgAMPCPP, an MgATP analogue and dead-end inhibitor (Figures 2b and 3b). The results of the thermodynamic analysis are summarized in Table 1. The values of all the dissociation constants for mutants R82A and R92A were similar to those for the wild-type HPPK. The largest difference was a less than 2-fold increase in the dissociation constant of AMP for R92A in comparison with that of the wild-type HPPK.

*Stopped-Flow Analysis*. The assembly of the ternary Michaelis complex involves large conformational changes in HPPK, especially in loop 3 that begins with R82 and ends with R92 (*9*). Thus, it is of interest to investigate the effects of the mutations on the kinetics of the binding of the substrates. In the case of the wild-type HPPK, the binding kinetics for MgATP was measured by the change in the fluorescence of the enzyme by stopped-flow analysis and that for HP by the change in the fluorescence of the ligand (*14*). The fluorescent change caused by the binding of MgATP was small but sufficient for measuring the binding kinetics. The same procedures were used for R92A (Figure 4). The results are summarized in Table 2. The rate constants for the binding of MgATP to R92A were very similar to those for the binding to the wild-type HPPK. But the rate constants for the binding of HP were significantly smaller than those for the binding to the wild-type HPPK. The forward rate constant decreased by a factor of ~4.5 and the reverse rate constant by a factor of 10.

The kinetics of the binding of HP to R82A could be measured with the same procedure as that for the wild-type HPPK (Figure 5b), but the fluorescent change caused by the binding of MgATP to R82A was too small for accurate measurement of the binding kinetics. However, we could measure the binding kinetics of MgAMPCPP by monitoring

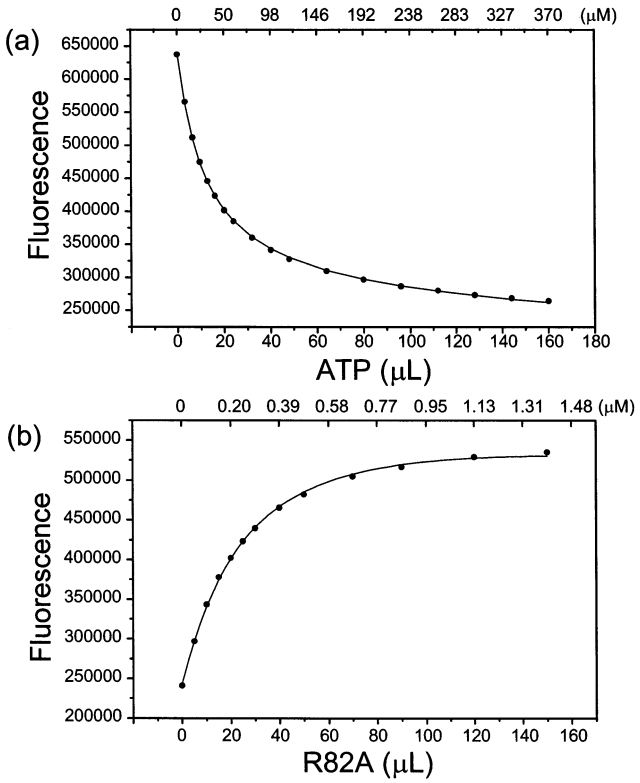


FIGURE 2: Equilibrium binding properties of R82A measured by fluorometry. (a) A 2 mL solution containing 10 $\mu$M R82A and 10 $\mu$M Ant-ATP in 100 mM Tris-HCl and 10 mM $MgCl_2$, pH 8.3 was titrated with ATP by adding aliquots of a 5 mM ATP stock solution at 24 °C. The top axis indicates the concentrations of ATP during the titration. The solid line was obtained by nonlinear least-squares fit to eq 1 as described under Experimental Procedures. (b) A 2 mL solution containing 0.11 $\mu$M HP and 100 $\mu$M AMPCPP in 100 mM Tris-HCl, 10 mM $MgCl_2$, and 25 mM DTT, pH 8.3 was titrated with R82A by adding aliquots of a 20 $\mu$M R82A stock solution at 24 °C. The top axis indicates the concentrations of R82A during the titration. The solid line was obtained by nonlinear least-squares fit to eq 2 as described under Experimental Procedures.

the fluorescent change of HP. Binding of MgAMPCPP and HP follows an ordered process with MgAMPCPP binding first. When HPPK is incubated first with MgAMPCPP and then mixed with HP, the fluorescent change allows the measurement of the kinetics of the binding of HP. When HPPK is mixed with MgAMPCPP and HP at the same time, the fluorescent change reflects the kinetics of the binding of both MgAMPCPP and HP. Because we already measured the rate constants for the binding of HP, and the values of these rate constants were significantly different from those for the binding of MgAMPCPP, we could precisely measure the rate constants for the binding of MgAMPCPP. The forward rate constant for the binding of MgAMPCPP to the wild-type HPPK was 0.3 $\mu M^{-1}$ $s^{-1}$, very similar to that for the binding of MgATP. But the reverse rate constant for the binding of MgAMPCPP was much smaller than that for the binding of MgATP, reflecting the higher affinity of MgAMPCPP for HPPK. The rate constants for the binding of MgAMPCPP (Figure 5a) and HP (Figure 5b) to R82A were comparable to those for the binding to the wild-type HPPK (Table 2).

*Quench-Flow Analysis*. The catalytic properties of the mutants were measured by quench-flow analysis. Previously, we showed that the reaction catalyzed by the wild-type HPPK

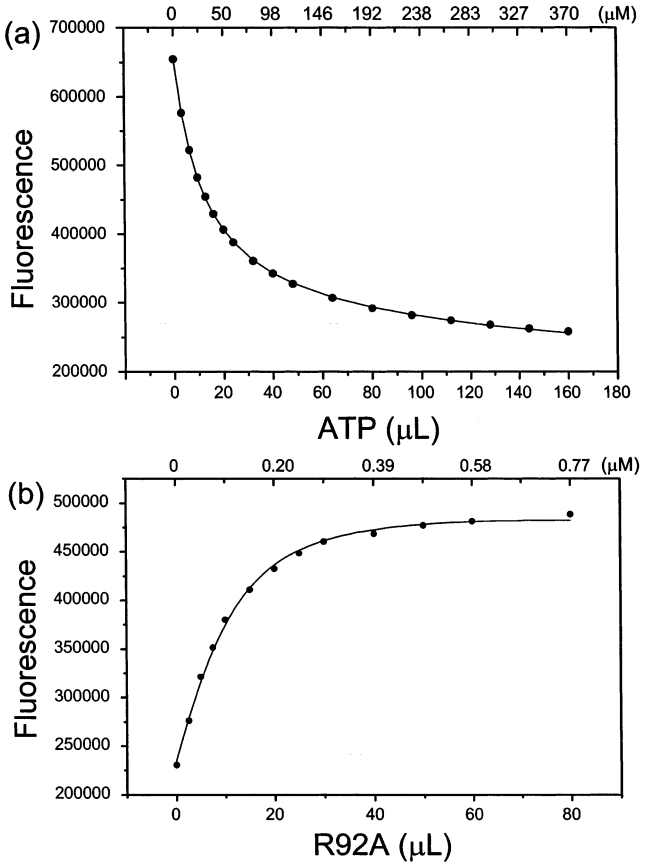


FIGURE 3: Equilibrium binding properties of R92A measured by fluorometry. (a) A 2 mL solution containing 10 $\mu$M R92A and 10 $\mu$M Ant-ATP in 100 mM Tris-HCl and 10 mM $MgCl_2$, pH 8.3 was titrated with ATP by adding aliquots of a 5 mM ATP stock solution at 24 °C. The top axis indicates the concentrations of ATP during the titration. The solid line was obtained by nonlinear least-squares fit to eq 1 as described under Experimental Procedures. (b) A 2 mL solution containing 0.11 $\mu$M HP and 100 $\mu$M AMPCPP in 100 mM Tris-HCl, 10 mM $MgCl_2$, and 25 mM DTT, pH 8.3 was titrated with R92A by adding aliquots of a 20 $\mu$M R92A stock solution at 24 °C. The top axis indicates the concentrations of R92A during the titration. The solid line was obtained by nonlinear least-squares fit to eq 2 as described under Experimental Procedures.

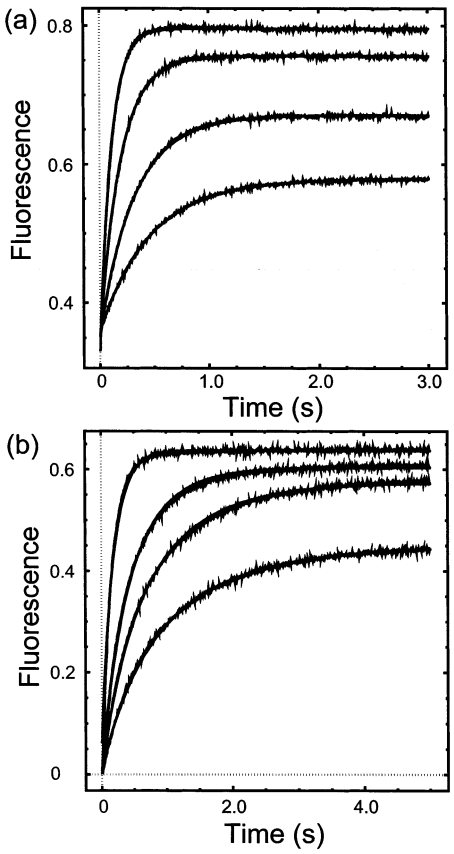


FIGURE 4: Stopped-flow analysis of the binding of MgATP (a) and HP (b) to R92A. (a) The concentrations of HPPK and $MgCl_2$ were fixed at 2 $\mu$M and 10 mM, respectively. The concentrations of ATP were 5, 10, 20, and 40 $\mu$M for traces from bottom to top, respectively. (b) The concentrations of HPPK, AMPCPP, and $MgCl_2$ were fixed at 0.25 $\mu$M, 30 $\mu$M, and 10 mM, respectively. The concentrations of HP were 0.25, 0.5, 1, and 2 $\mu$M for traces from bottom to top, respectively. All concentrations refer to the concentrations right after the rapid mixing. The solid lines were obtained by global fitting using the program DYNAFIT (*19*).

follows classical burst kinetics, and the rate-limiting step is product release (*14*). Initial quench-flow analysis of R92A also showed burst kinetics (data not shown). We attributed the burst kinetics to the contamination of the wild-type HPPK because the rate constant for the linear phase was extremely low, the *Escherichia coli* strain BL21(DE3) used to produce the mutant proteins contained a wild-type gene for HPPK in its chromosome, and the same procedure was used for the purification of the wild-type and the mutant proteins. The contamination was rather small and estimated to be <0.1% based on the levels of the expression of the genes, but it was sufficient to dominate the kinetics because the mutant had an extremely low catalytic activity. The minute contamination, however, did not have any significant effects on the measurements of the ligand-binding properties of the mutant.

To eliminate the contamination of the wild-type HPPK encoded by the chrosomal gene, plasmid constructs were made by fusing the HPPK gene to the gene encoding GST. The fusion proteins were purified by affinity chromatography with a glutathione agarose column, thus eliminating the wild-type HPPK produced by the chrosomal gene. The GST moiety was removed by thrombin cleavage, leaving the protein with four extra residues Gly−Ser−His−Met at the N-terminus (the N-terminal methionine is removed in the native HPPK). The kinetics of the cleaved protein (WT*, Figure 6) was very similar to that of the native HPPK. The time course consists of two phases, a burst phase and a steady-state phase as described by eq 4. The burst phase is characterized by two constants, the amplitude A and the rate constant $\lambda$. The steady-state phase is characterized by the rate constant $k_{cat}$. The three constants are related to the rate constants in Figure 1 according to the following equations (*21*):

$$A = \frac{k_3(k_3 + k_{-3})}{(k_3 + k_{-3} + k_4)^2} \quad (5)$$

$$\lambda = k_3 + k_{-3} + k_4 \quad (6)$$

$$k_{cat} = \frac{k_3 k_4}{k_3 + k_{-3} + k_4} \quad (7)$$

The amplitude and rate constants for the two phases of the reaction were evaluated by nonlinear least-squares fit to eq 4. The individual rate constants were then estimated accord-

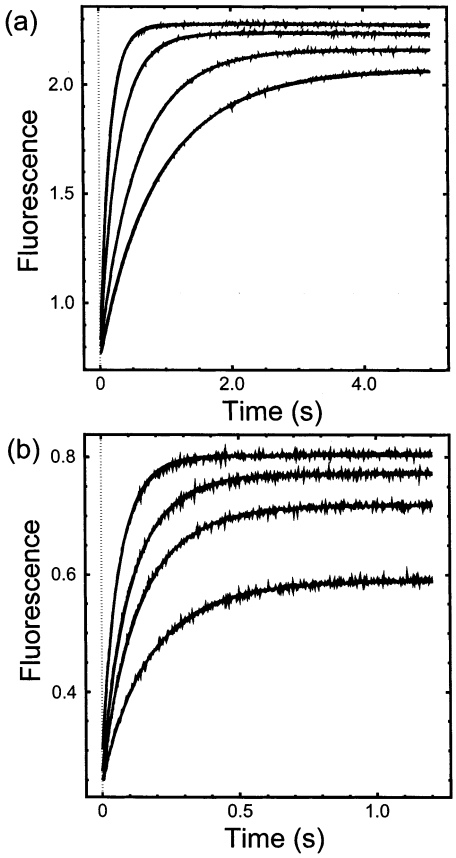


FIGURE 5: Stopped-flow analysis of the binding of MgAMPCPP (a) and HP (b) to R82A. (a) The concentrations of HPPK, HP, and $MgCl_2$ were fixed at 2 $\mu$M, 20 $\mu$M, and 10 mM, respectively. The concentrations of AMPCPP were 5, 7.5, 20, and 40 $\mu$M for traces from bottom to top, respectively. (b) The concentrations of HPPK, AMPCPP, and $MgCl_2$ were fixed at 0.25 $\mu$M, 30 $\mu$M, and 10 mM, respectively. The concentrations of HP were 0.25, 0.5, 1, and 2 $\mu$M for traces from bottom to top, respectively. All concentrations refer to the concentrations right after the rapid mixing. The solid lines were obtained by global fitting using the program DYNAFIT (*19*).

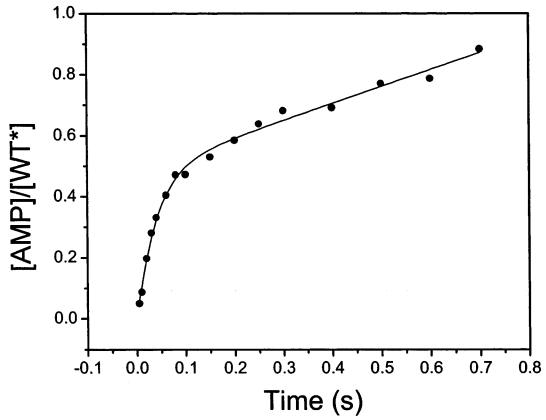


FIGURE 6: HPPK burst kinetics. The reaction mixture contained 10 $\mu$M WT* (wild-type HPPK with four extra residues Gly−Ser−His−Met at the N-terminus), 100 $\mu$M ATP, 110 $\mu$M HP, 25 mM DTT, 0.5 mM EDTA, and 10 mM $MgCl_2$ in 100 mM Tris-HCl buffer, pH 8.3. The reaction was initiated by mixing with $MgCl_2$ at 30 °C and quenched by mixing with EDTA. The solid lines were obtained by nonlinear least-squares fit to eq 4 as described under Experimental Procedures.

ing to eqs 5−7 and used to set the initial values for the numerical analysis using the program DYNAFIT (*19*). The values for the individual rate constants are listed in Table 2.

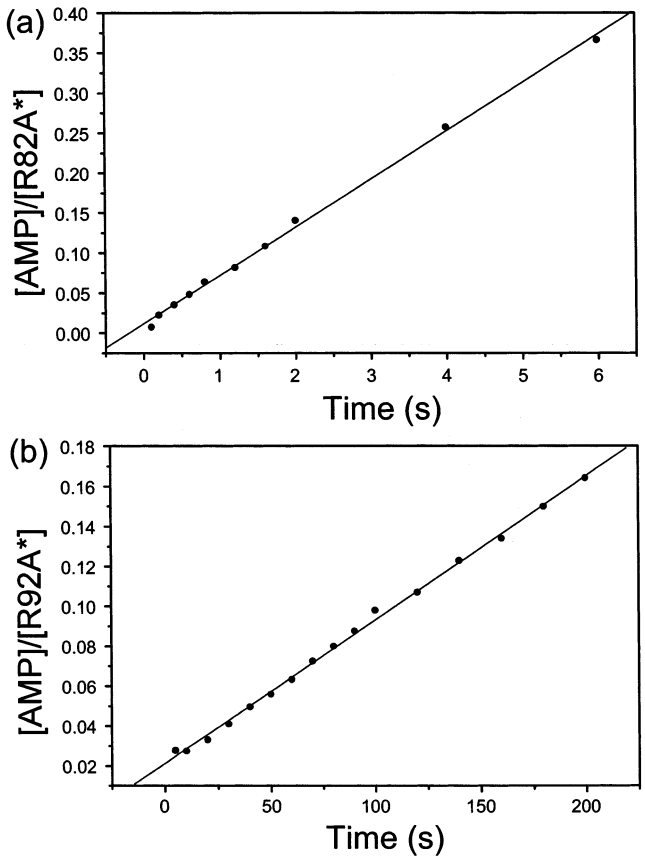


FIGURE 7: Quench-flow analysis of R82A* (a) and R92A* (b). The asterisks indicate four extra residues Gly−Ser−His−Met at the N-termini of the mutants. Ten $\mu$M R82A* or R92A* was used in the experiments, and the other experimental conditions were the same as described in Figure 6. The solid lines were obtained by linear least-squares regression.

The $k_{cat}$ values were calculated according to eq 7 and are also listed in Table 2. The results showed that both GSTHPPK and WT* have very similar catalytic properties to that of the native wild-type HPPK.

R82A* and R92A* (with four extra residues Gly−Ser−His−Met at the N-terminus) were produced by the same procedure for HPPK*. The results of the quench-flow analysis of R82A* and R92A* are shown in Figure 7. No burst kinetics was observed for either R82A or R92A, indicating that the chemical step is rate limiting in the reaction catalyzed by either mutant. The rate constants obtained by least-squares linear regression were 0.066 $s^{-1}$ for R82A* and 7.2 $\times$ $10^{-4}$ $s^{-1}$ for R92A*, respectively. Because the chemical step was rate limiting in the reaction catalyzed by R82A* or R92A*, these rate constants for the mutants were for the chemical step rather than for the product release as in the wild-type HPPK. Therefore, the substitution of R82 with alanine caused a decrease in the rate constant for the chemical step by a factor of ~380 (25 $s^{-1}$ for WT* vs 0.066 $s^{-1}$ for R82A*), and the substitution of R92 with alanine caused a decrease in the rate constant for the chemical step by a factor of ~3.5 $\times$ $10^4$ (25 $s^{-1}$ for WT* vs 7.2 $\times$ $10^{-4}$ $s^{-1}$ for R92A*).

## DISCUSSION

By site-directed mutagenesis and detailed thermodynamic and kinetic analyses of the mutants, we have shown that both

R82 and R92 are important in HPPK catalysis but play only minor roles in the binding of the substrates. Mutation of either residue causes a shift of the rate-limiting step in the reaction. The wild-type HPPK shows a classical burst kinetic behavior (Figure 6), and the rate-limiting step is the release of products rather than the chemical transformation (*14*). In contrast, both R82A and R92A show no burst kinetics (Figure 7), indicating that the chemical step is rate-limiting in the reaction catalyzed by the two HPPK mutants, and the rate constant for the chemical step is very close to $k_{cat}$. The substitution of R82 by alanine causes a decrease in the rate constant for the chemical step by a factor of ~380, and the substitution of R92 by alanine causes a decrease in the rate constant by a factor of $\sim 3.5 \times 10^4$. The dramatic decreases in the catalytic power of the enzyme are apparently not because of conformational perturbations because the overall structures of both mutants are very similar to that of the wild-type HPPK (see the companion paper for the details of the structural analysis). The results taken together clearly show that R92 plays a critical role in the catalysis by HPPK and contributes 6.3 kcal/mol to the transition-state stabilization. Comparatively, R82 contributes less to the transition-state stabilization (3.6 kcal/mol).

While both R82 and R92 make substantial contributions to catalysis, their contributions to the binding of the substrates are small. R82 is dispensable for the binding of the substrates because substitution of R82 by alanine does not have any significant effect on the free energy or the kinetics of the binding of either substrate. R92 is not important for the binding of MgATP because substitution of R92 with alanine does not cause any significant change in the free energy of binding for MgATP or its kinetics. R92 does not contribute to the free energy of binding of HP because the $K_d$ of HP for R92A is very similar to that for the wild-type HPPK. But R92 is involved in the binding of HP and accelerates the formation of the HP complex because substitution of R92 with alanine decreases the rate constant for the formation of the HP complex by a factor of ~7 and the rate constant for the dissociation of the complex by a factor of ~16.

The contributions of R82 and R92 to catalysis as revealed by the thermodynamic and transient kinetic analyses of the mutants are consistent with the structural information on HPPK (see the companion paper for details). Two binding modes have been found for R82 and R92. In the structure of HPPK in complex with AMPCPP and HP (*9*), R92 forms two hydrogen bonds with the α-phosphate of AMPCPP, and R82 has no direct interaction with the nucleotide. In the structure of HPPK in complex with ATP and an HP analogue (*13*), R82 forms two hydrogen bonds with the α-phosphate of ATP and one hydrogen bond with the carboxylate of the conserved D95 that is coordinated with both bound $Mg^{2+}$ ions. R92 forms two hydrogen bonds with the β-phosphate of ATP. Both binding modes exist in our new structure at 0.89 Å resolution. It appears that the side chains of both R82 and R92 are rather dynamic in the catalytic cycle of HPPK. The guanidinium groups of both R82 and R92 point away from the active site in the unliganded form. R92 moves first to interact with the α-phosphate and then the β-phosphate of ATP. The guanidinium group of R82 can only move to interact with the α-phosphate of ATP, and its movement is roughly parallel to that of R92 (see the companion paper for details). The transition state structure is not known. The hydroxyl group of the bound pterin compound is well-positioned for an in-line nucleophilic attack on the β-phosphorus of the NTP (*9*). The angle formed by the hydroxyl oxygen of HP, the β-phosphorus, and the bridging methylene carbon in the structure of HPPK in complex with HP, AMPCPP, and $Mg^{2+}$ ions is 174.5°, very close to the ideal value of 180° for an in-line nucleophilic attack. The distance between the hydroxyl oxygen of HP and the β-phosphorus is only 3.2 Å, 1.7 Å shorter than the so-called reaction coordinate distance of 4.9 Å for a fully dissociate mechanism (*22*), suggesting that the reaction may have some associative character in the transition state. The fact that HPPK also catalyzes the hydrolysis of ATP to ADP and phosphate rather than AMP and pyrophosphate also supports an associative mechanism (*11*). A dissociative mechanism, however, cannot be ruled out. It is quite possible that the transition state is neither fully associative nor fully dissociative and is rather between the two extreme cases. Charge distributions in the two mechanisms are different and require different positioning of key catalytic groups (*23*). In an associative mechanism, the bond between the hydroxyl oxygen of HP and the β-phosphorus of ATP is largely formed, and the bond to the leaving group is largely intact; therefore, there is a gain of charge on the β-phosphoryl group in the transition state. In a dissociative mechanism, there is little bond formation between the hydroxyl oxygen of HP and the β-phosphorus of ATP, and the bond between the β-phosphorus of ATP and the leaving group is largely broken. Therefore, there is a loss of charge on the β-phosphoryl group and a gain of charge on the bridging oxygen between the α- and the β-phosphoryl groups. Regardless of which mechanism HPPK follows, R92 will be able to move to neutralize the negative charge developed at the transition state. On the other hand, R82 can only interact with the α-phosphoryl group. Thus, substitution of R92 with alanine causes a dramatic decrease, and substitution of R82 with alanine causes a moderate decrease in the catalytic power of HPPK.

The fact that substitution of R82 with alanine does not have any significant effects on the binding of MgATP is consistent with the structure of HPPK·HP·MgAMPCPP in which no direct interaction between the guanidinium group and AMPCPP is observed (*9*). Interestingly, although R92 interacts with α-, β-, or both phosphoryl groups, substitution of R92 with alanine does not have any significant effects on the binding of MgATP, either. Instead, it promotes both the binding and the dissociation of HP. The result suggests that R92 is not important for the binding of MgATP, yet it does not mean that R92 does not contribute to the binding of the nucleotide. As revealed by the crystal structure of R92A·HP·MgAMPCPP (see the companion paper for details), the loss of the interaction between the guanidinium group of R92 and AMPCPP is compensated by the moving in of the guanidinium groups of R82 and R84. The guanidinium group of R82 forms one hydrogen bond and that of R84 forms two hydrogen bonds with the α-phosphate. The biochemical and structural data suggest that R92 is involved in but dispensable for the binding of MgATP. The effects of the R92 mutation on the kinetics of HP binding is probably due to the coupling between the three catalytic loops (*9*). The assembling of the catalytic center of HPPK involves dramatic conformational changes of the three catalytic loops. Of the three loops, loop 2 is directly involved in the binding of HP, but the movement

of loop 2 is coupled to loop 3 where R92 resides. Therefore, R92 also plays a role in facilitating the binding of HP and the assembling of the ternary complex.

## REFERENCES


1. Shiota, T. (1984) in *Chemistry and Biochemistry of Folates* (Blakley, R. T., and Benkovic, S. J., Eds.) pp 121−134, John Wiley & Sons, New York.
2. Blakley, R. L., and Benkovic, S. J. (1984) *Folates and Pterins*, John Wiley & Sons, New York.
3. Switzer, R. L. (1974) in *The Enzymes* (Boyer, P., Ed.) pp 607−629, Academic Press, New York.
4. Mildvan, A. S., Weber, D. J., and Abeygunawrdana, C. (1999) *Adv. Enzymol. Relat. Areas Mol. Biol. 73*, 183−207.
5. Eriksen, T. A., Kadziola, A., Bentsen, A. K., Harlow, K. W., and Larsen, S. (2000) *Nat. Struct. Biol. 7*, 303−308.
6. Baker, L. J., Dorocke, J. A., Harris, R. A., and Timm, D. E. (2001) *Structure 9*, 539−546.
7. Timm, D. E., Liu, J. Y., Baker, L. J., and Harris, R. A. (2001) *J. Mol. Biol. 310*, 195−204.
8. Xiao, B., Shi, G., Chen, X., Yan, H., and Ji, X. (1999) *Structure 7*, 489−496.
9. Blaszczyk, J., Shi, G., Yan, H., and Ji, X. (2000) *Structure 8*, 1049−1058.
10. Shi, G., Blaszczyk, J., Ji, X., and Yan, H. (2001) *J. Med. Chem. 44*, 1364−1371.
11. Xiao, B., Shi, G., Gao, J., Blaszczyk, J., Liu, Q., Ji, X., and Yan, H. (2001) *J. Biol. Chem. 276*, 40274−40281.
12. Hennig, M., Dale, G. E., D'Arcy, A., Danel, F., Fischer, S., Gray, C. P., Jolidon, S., Müller, F., Page, M. G. P., Pattison, P., and Oefner, C. (1999) *J. Mol. Biol. 287*, 211−219.
13. Stammers, D. K., Achari, A., Somers, D. O., Bryant, P. K., Rosemond, J., Scott, D. L., and Champness, J. N. (1999) *FEBS Lett. 456*, 49−53.
14. Li, Y., Gong, Y., Shi, G., Blaszczyk, J., Ji, X., and Yan, H. (2002) *Biochemistry 41*, 8777−8783.
15. Thijssen, H. H. W. (1973) *Anal. Biochem. 54*, 609−611.
16. Scrimgeour, K. G. (1980) *Methods Enzymol. 66*, 517−523.
17. Shi, G., Gong, Y., Savchenko, A., Zeikus, J. G., Xiao, B., Ji, X., and Yan, H. (2000) *Biochim. Biophys. Acta 1478*, 289−299.
18. Wang, Z.-X. (1995) *FEBS Lett. 360*, 111−114.
19. Kuzmic, P. (1996) *Anal. Biochem. 237*, 260−273.
20. Bermingham, A., Bottomley, J. R., Primrose, W. U., and Derrick, J. P. (2000) *J. Biol. Chem. 275*, 17962−17967.
21. Johnson, K. A. (1992) in *The Enzymes* (Sigman, D. S., Ed.) pp 1−61, Academic Press, San Diego.
22. Mildvan, A. S. (1997) *Proteins 29*, 401−416.
23. Maegley, K. A., Admiraal, S. J., and Herschlag, D. (1996) *Proc. Natl. Acad. Sci. U.S.A. 93*, 8160−8166.


BI026800Z